Control Engineering Practice 69 (2017) 23–35

Contents lists available at ScienceDirect

Control Engineering Practice

journal homepage: www.elsevier.com/locate/conengprac

Modeling and robust control of a twin wind turbines structure

I. Guenoune [a,b], F. Plestan [a,*], A. Chermitti [b], C. Evangelista [c]

[a] École Centrale de Nantes-LS2N, Nantes, France
[b] Université de Tlemcen-LAT, Tlemcen, Algeria
[c] LEICI, UNLP-CONICET, La Plata, Argentina

ARTICLE INFO

Keywords:
Wind turbine
Nonlinear system
Robust control
Sliding mode controller (SMC)

ABSTRACT

The control of a new structure of twin wind turbines (TWT) is presented in this paper. This new concept includes two identical wind turbines ridden on the same tower, which can pivot face the wind with no additional actuator. The motion of the arms carrying the TWT is free. The control law based on sliding mode controller is designed to track the maximum power, by controlling the rotor speed of the TWT and the yaw rotation but without yaw actuator. Finally, performances of the proposed control strategy are compared to standard proportional integral controller, for several scenarios (time varying direction or magnitude of the wind, error on the inertia of the system, ...).

1. Introduction

An original new structure of twin wind turbines is presented in this work. This concept named SEREO and patented by Herskovits, Laffitte, Thome, and Tobie (2012) (see Fig. 1) includes two identical wind turbines ridden on the same tower, which can pivot in front of the wind.

The original feature of SEREO versus standard twin turbines is due to the fact that the rotation of the arms carrying the two wind turbines is free: indeed, no additional yaw driving motor is required to follow the wind direction which is really a novelty. The challenge is to design a control structure to force the system against the wind while ensuring optimal energy production. The advantages of such structure are

- Given that there is no yaw actuation, failures risks are reduced, as well as maintenance ;
- Furthermore, on a same tower, two turbines are available. For a given nominal power for the whole system, especially for the large power turbines (>10 MW), it is more interesting by a weight point-of-view to have two turbines, than only a single one.

However, as previously mentioned, it is necessary to design an appropriate control strategy to align the turbines face the wind. Concerning the electrical part of the system, the two wind turbines are associated with two permanent magnet synchronous generators.

In order to reach a high efficiency, two objectives have to be managed: the first one consists in controlling the position of the wind turbine with respect to the wind direction whereas the second controller is devoted to the electrical generator. The rotor speed of the wind turbine is controlled by maintaining the tip speed ratio at its optimum value (Corradini, Ippoliti, & Orlando, 2013; Huang, Li, Ding, Jin, & Ma, 2015a; Saravanakumar & Jena, 2015). For this objective, various control strategy have been introduced, such as direct torque control (DTC) and oriented field control (Chinchilla, Arnaltes, & Burgos, 2006; Zhang, Zhao, Qiao, & Qu, 2014). It means that the angular velocity of the wind turbine has to be controlled with respect to the velocity and the direction of the wind. In fact, the wind turbine is the most efficient if it is face the wind. In the framework of the power maximization by following the wind direction, it is worth mentioning (Mesemanolis & Mademlis, 2014), where the MPPT (Maximum Power Point Tracking) technique is combined with the active yaw control. The misalignment angle between the nacelle and the wind direction is estimated from the optimum and real mechanical power. It means that no sensor is required for the wind direction. The yaw control can be also used to protect the wind turbine against the excess power at high wind speed (Shariatpanah, Fadaeinedjad, & Rashidinejad, 2013).

For SEREO concept, the difficulty is that there is no yaw actuator. It is shown in the sequel that, viewed that there are two wind turbines, a difference between the drag forces of the turbines is created to unbalance the yaw trim. The control of the yaw angle allows to maintain this structure in front of the wind. Indeed, by varying the pitch angle of the two wind turbines, a different of the aerodynamic forces is created

* Corresponding author.
E-mail address: franck.plestan@ec-nantes.fr (F. Plestan).

http://dx.doi.org/10.1016/j.conengprac.2017.08.009
Received 20 March 2017; Received in revised form 17 August 2017; Accepted 18 August 2017
0967-0661/

Fig. 1. SEREO structure (Herskovits et al., 2012) composed of twin wind turbines.

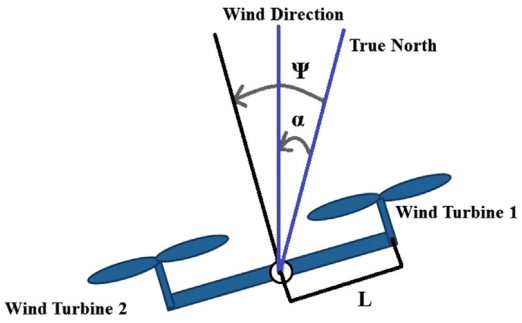

Fig. 2. Simplified model of the twin wind turbines (view from the top).

between the two rotors. Thus, the torque resulting from this difference enables to drive the yaw rotation of the structure around the vertical axis.

The SEREO system including mechanical and electrical parts, is a nonlinear system where it is greatly disturbed (wind variations, parametric uncertainties, ...). Furthermore, the variable speed-variable pitch wind turbines are expected to operate in large scale of the wind velocity (Huang et al., 2015a; Tan, Thanh, & Dong, 2015). Due to these features, it is crucial to develop control laws which are robust with respect to uncertainties and perturbations, and which are efficient over a large operating domain. In the framework of the control design, the standard proportional integral PI controller is widely used in industrial context for different applications, and also for wind turbines (Chen, Chen, & Gong, 2013; Ikni, Camara, Camara, Dakyo, & Gualous, 2014; Zaragoza, Pou, Arias, Spiteri, Robles, et al., 2011). However, the PI controller is considered as a linear controller; therefore, an accurate knowledge of the system is required to ensure a good performance (Corradini et al., 2013) and the operating domain of the controller is quite limited. It means that, outside this domain, the control strategy is less efficient in terms of accuracy, disturbance rejection and parametric variations.

Several nonlinear control strategies have been used in order to overcome the drawbacks of robustness and limited operating domain. Thus, one can cite fuzzy-sliding mode control (Yan, Lin, Feng, Guo, Huang, et al., 2012) or adaptive neural network (Jafarnejadsani, Pieper, & Ehlers, 2013) which are quite efficient but are not easy to tune and formally implement. Concerning robust nonlinear control, integral sliding mode control has been used in Saravanakumar and Jena (2015) to control the wind turbines in three different regions (optimizing the power, limiting the power, and transient region for loads transient reducing).

The choice in the current work has been to develop sliding mode based control. This approach (Shtessel, Edwards, Fridman, & Levant, 2014; Utkin, Guldner, & Shi, 1999) is known to be robust versus parametric uncertainties and perturbations, quite easy to tune and has been used in numerous fields of application (Fridman, Barbot, & Plestan, 2016; Girin, Plestan, Brun, & Glumineau, 2009; Utkin, 1993; Utkin et al., 1999) including wind turbines area (Beltran, Ahmed-Ali, & Benbouzid, 2008, 2009).

The main objective of this work is then to propose, for the first time, a control architecture for a twin turbines structure without yaw actuation in order to optimize the power production. The main contributions are

- Nonlinear model of the SEREO twin wind turbines structure (dynamics of the yaw of the structure, the rotation velocities of turbines, and the direct/quadratic currents of the generator),
- Control of the both mechanical and electrical parts of SEREO structure, based on sliding mode approach,
- Evaluation of the closed-loop system performances under different scenarios (structure face the wind, structure not face the wind, parametric uncertainties, ...),

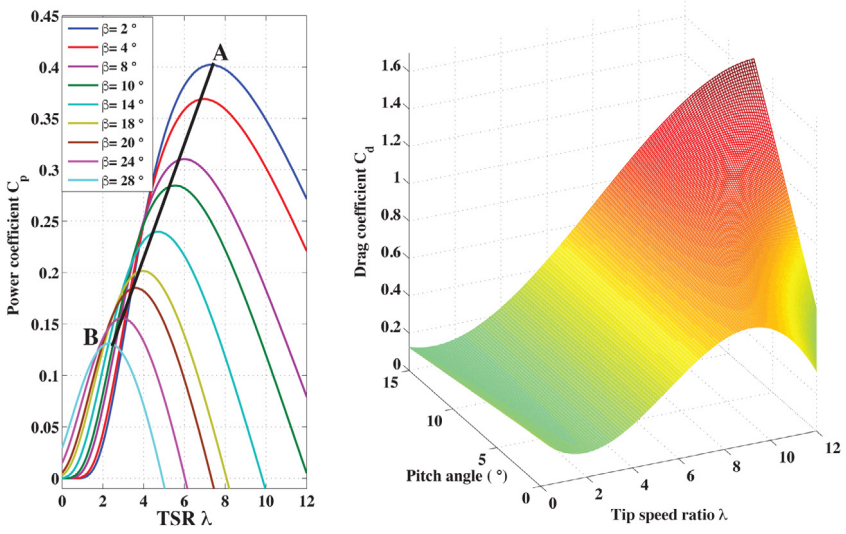

Fig. 3. Left (a)—Power coefficient C_p versus the tip-speed ratio λ, for different values of pitch angle. Right (b)—Drag coefficient C_d versus the tip-speed ratio λ and the pitch angle β. (For interpretation of the references to color in this figure legend, the reader is referred to the web version of this article.)

- Performances comparison (standard deviation of the electromagnetic torques and the mean power) of the proposed approach control strategy (SMC) versus standard proportional integral one (PI).

The paper is organized as follows. In Section 2, the nonlinear model of the TWT including the mechanical and electrical parts is introduced. Control problem is stated in Section 3. Then, a robust control scheme based on sliding mode concept is detailed in Section 4. Section 5 discusses the simulation results for four different scenarios, and Section 6 presents conclusion and future work.

2. Modeling of the SEREO structure

The SEREO structure (Herskovits et al., 2012) is a floating innovative structure of twin wind turbines (see Fig. 1); in this paper, the SEREO structure is supposed to be located on the ground. The main innovation of a such structure is that the rotation around its vertical axis, that allows to force the turbines face the wind, is not actuated (which is a break point with respect to standard wind turbines with similar power (2 MW)). It simplifies maintenance, and reduces the cost of the structure. However, it induces that the control of the wind turbines has to include the orientation of the structure face the wind, whereas it has also to guarantee optimal electrical power production. A such controller is displayed in the next section.

In this section, a full model of the SEREO structure is detailed and composed of the aerodynamic model, pitch angle dynamics, yaw dynamics, and angular velocities/direct-quadratic currents dynamics of the generators.

2.1. Aerodynamic and mechanical model

Fig. 2 displays a scheme of the SEREO structure, viewed from the top. One supposes that the two turbines have the same features. In the rest of the paper, the twin turbines are denoted with an index i, such that $i \in \{1,2\}$, which gives Turbine 1 and Turbine 2. From Fig. 2, α (resp. ψ) is the angle between the True North and the wind direction (resp. the orientation of the wind turbines defined by an axis that is perpendicular to the arm connecting the two turbines).

The mechanical power P_{ai} captured by each turbine from the wind, the aerodynamic torque Γ_{ai} and the drag force F_{di} are given by ($i \in \{1,2\}$)

$$\begin{aligned} P_{ai} &= \frac{1}{2} C_{p,i}(\lambda_i,\beta_i)\,\rho\,\pi\,R^2\,(V\cos(\psi-\alpha))^3 \\ \Gamma_{ai} &= \frac{1}{2}\frac{C_{p,i}(\lambda_i,\beta_i)}{\lambda_i}\,\rho\,\pi\,R^3\,(V\cos(\psi-\alpha))^2 \\ F_{di} &= \frac{1}{2} C_{d,i}(\lambda_i,\beta_i)\,\rho\,\pi\,R^2\,(V\cos(\psi-\alpha))^2 \end{aligned} \tag{1}$$

with R the radius of the wind turbines blades, ρ the air density, V the wind velocity, β_i the pitch angle of the blades, and λ_i the tip-speed ratio (TSR) which is defined as

$$\lambda_i = \frac{\Omega_i}{V\cos(\psi-\alpha)}\,R. \tag{2}$$

The power coefficient $C_{p,i}$ depends on the TSR and the pitch angle (Huang et al., 2015a; Uehara, Pratap, Goya, Senjyu, Yona et al., 2011) and reads as

$$C_{p,i}(\lambda_i,\beta_i) = c_1\,(c_2\,a - c_3\,\beta_i - c_4)\,e^{-c_5\,a} \tag{3}$$

with

$$a = \frac{1}{\lambda_i + 0.08\,\beta_i} - \frac{0.035}{\beta_i^3+1},$$

and

$$c_1 = 0.22, \quad c_2 = 116, \quad c_3 = 0.4, \quad c_4 = 12.5, \quad c_5 = 21.$$

Fig. 3-Left displays the evolution of the power coefficient versus the TSR, for different values of the pitch angle of the blades. As detailed in the control section, the objective consists in producing the maximal electrical power: it means that the system must be controlled to get a maximal value of $C_{p,i}$. It means also that the pitch angle, β_i and the TSR, λ_i have to be adjusted to reach this objective. The black bold curve (AB) (Fig. 3-Left) corresponds to the optimal power coefficient. Along this curve, by applying the MPPT (Maximum Point Power Tracking) strategy (Beltran et al., 2008), the wind turbine operates in high efficiency to produce the maximal energy. Finally, this *optimal* curve allows to link the tip-speed ratio λ_i and an *optimal* pitch angle β_i^{opt}, which corresponds to an *optimal* value of power coefficient $C_{p,i}^{opt}$ (Eberhart, Chung, Haumer, & Kral, 2015; Tang, Guo, & Jiang, 2011): this link is given by the following function

$$\begin{aligned} \beta_i^{opt} &= 0.0219\,\lambda_i^4 - 0.2810\,\lambda_i^3 + 0.4421\,\lambda_i^2 \\ &\quad + 11.8415\,\lambda_i - 7.9378. \end{aligned} \tag{4}$$

The drag coefficient $C_{d,i}$ (Georg, Schulte, & Aschemann, 2012) is a nonlinear function of the TSR and the pitch angle. From Georg et al. (2012), a least squares polynomial interpolation method allows to get an expression of $C_{d,i}$ that reads as

$$\begin{aligned} C_{d,i}(\lambda_i,\beta_i) &= \underbrace{a_0 + a_1\,\lambda_i + a_2\,\lambda_i^2 + a_3\,\lambda_i^3}_{\mathcal{A}_i} \\ &\quad + \underbrace{\left(b_0 + b_1\,\lambda_i + b_2\,\lambda_i^2 + b_3\,\lambda_i^3\right)}_{\mathcal{B}_i}\cdot\beta_i \end{aligned} \tag{5}$$

with $a_0 = 0.25382$, $a_1 = -0.1369$, $a_2 = 0.04345$, $a_3 = -0.00263$, $b_0 = -0.008608$, $b_1 = 0.0063$, $b_2 = -0.0015$ and $b_3 = 0.000118$.

2.2. Blade pitch dynamics

As mentioned previously, the blade pitch angles β_1 and β_2 can be modified, in order to modify the drag forces F_{d1} and F_{d2} allowing to force the rotation of the SEREO structure. The dynamics of the pitch angles actuators of the two wind turbines can be written as a first order system (Huang, Li, & Jin, 2015b; Tan et al., 2015)

$$\begin{aligned} \dot{\beta}_1 &= \frac{1}{T_{\beta_1}}\beta_1^* - \frac{1}{T_{\beta_1}}\beta_1 \\ \dot{\beta}_2 &= \frac{1}{T_{\beta_2}}\beta_2^* - \frac{1}{T_{\beta_2}}\beta_2, \end{aligned} \tag{6}$$

with $T_{\beta_1} = T_{\beta_2}$ being the time constants of the blades actuation system and β_1^*, β_2^* the pitch angles references. The formulation of the model (6) supposes that there is an inner loop for the control of both pitch angles: the static gain equals 1, *i.e.,* the positioning is ideal, only the response time is taken into account through the time constants T_{β_1}, T_{β_2}. Of course, all the challenge consists in determining the values of β_1^* and β_2^* in order to ensure an optimal behavior of the system. The control strategy will be detailed in the sequel; however, some elements are given here to introduce definitions of β_1^* and β_2^*.

Definition of pitch angles references β_1^* and β_2^*. The wind turbines have to be face the wind to produce maximal energy: in this case, the control strategy will force the both ones to have the same angular velocities (in magnitude) in order to stabilize the structure face the wind.

However, by a practical point-of-view, it is not possible to have Ω_1 and Ω_2 with strictly the same magnitude. From (4), one gets, for the both wind turbines, the optimal values of the pitch angles denoted β_1^{opt} and β_2^{opt}. In this case, *i.e.,* if the structure is face the wind, one has

$$\begin{aligned} \beta_1^* &= \beta_1^{opt} \\ \beta_2^* &= \beta_2^{opt}. \end{aligned} \tag{7}$$

If the wind direction is changing, it is necessary to generate a difference between the drag forces F_{d1} and F_{d2}, by acting on the pitch angles and their references. Then, the pitch angles references β_1^* and β_2^* become

$$\begin{aligned}\beta_1^* &= \beta_1^{opt} + \Delta\beta_1 \\ \beta_2^* &= \beta_2^{opt} + \Delta\beta_2\end{aligned} \tag{8}$$

with β_1^{opt}, β_2^{opt} defined from (4) and $\Delta\beta_1$ and $\Delta\beta_2$ being viewed as the control inputs controlling the rotation of the structure.

2.3. Yaw dynamics

The dynamics of the rotation of the SEREO structure around its vertical axis is given by

$$K_r\ddot{\psi} = -D_r\dot{\psi} + (F_{d1} - F_{d2})\, L \tag{9}$$

with K_r and D_r the inertia moment and the friction coefficient, respectively, associated to yaw motion, and L the length between the horizontal axis and the vertical axis (Fig. 2). From (1)–(5), one gets

$$\begin{aligned}F_{d1} - F_{d2} &= \frac{1}{2}\rho\pi(RV\cos(\psi-\alpha))^2\left(C_{d,1} - C_{d,2}\right) \\ &= \frac{1}{2}\rho\pi(RV\cos(\psi-\alpha))^2\left[\mathcal{A}_1 - \mathcal{A}_2\right. \\ &\quad \left. + \mathcal{B}_1\cdot\beta_1 - \mathcal{B}_2\cdot\beta_2\right].\end{aligned} \tag{10}$$

Define $\varphi(\psi,\beta_1,\beta_2,\lambda_1,\lambda_2)$ as (with $C = \frac{1}{2}\rho\pi(RV\cos(\psi-\alpha))^2$)

$$\varphi = C\left[\mathcal{A}_1 - \mathcal{A}_2 + \mathcal{B}_1\cdot\beta_1 - \mathcal{B}_2\cdot\beta_2\right]. \tag{11}$$

2.4. Electrical model

The Permanent Magnet Synchronous Generator is widely used for the industrial applications (automobiles, conversion energy system), thanks to their high efficiency and large torque current ratio (Hamida, de Leon Morales, Glumineau, & Boisliveau, 2013). Its standard mathematical model, in the synchronous reference frame (d,q) is given by Glumineau and de Leon-Morales (2015) and Munteanu, Bratcu, Cutululis, and Emil (2008)

$$\begin{aligned}\dot{i}_{di} &= \frac{-R_s}{L_d}i_{di} + \frac{pL_q}{L_d}\Omega\, i_{qi} + \frac{1}{L_d}V_{di} \\ \dot{i}_{qi} &= \frac{-R_s}{L_q}i_{qi} - \frac{pL_d}{L_q}\Omega\, i_{di} - \frac{p\phi_f}{L_q}\Omega_i + \frac{1}{L_q}V_{qi} \\ \dot{\Omega}_i &= \frac{1}{J}\Gamma_{ai} - \frac{p[(L_d - L_q)i_{di} + \phi_f]}{J}i_{qi} - \frac{f_v}{J}\Omega_i\end{aligned} \tag{12}$$

where $i_{di}, i_{qi}, V_{di}, V_{qi}$ are respectively the stator currents and stator voltages, L_d, L_q are the dq-axis inductances, R_s is the stator resistance, p is the number of pole pairs, ϕ_f permanent-magnet flux linkage, J is the total inertia, and f_v the friction coefficient.

2.5. Nonlinear model of the SEREO system

The SEREO system can be written as a nonlinear system affine with respect to the control input vector

$$\dot{x} = f(x) + g(x)\cdot u \tag{13}$$

with x the state vector and u the input vector respectively defined as

$$\begin{aligned}x &= \left[\beta_1\ \ \beta_2\ \ \psi\ \ \dot{\psi}\ \ i_{d1}\ \ i_{q1}\ \ \Omega_1\ \ i_{d2}\ \ i_{q2}\ \ \Omega_2\right]^T, \\ u &= \left[\beta_1^*\ \ \beta_2^*\ \ V_{d1}\ \ V_{q1}\ \ V_{d2}\ \ V_{q2}\right]^T.\end{aligned} \tag{14}$$

The vector $f(x)$ and the matrix $g(x)$ read as

$$f(x) = \begin{bmatrix}
-\frac{1}{T_{\beta1}}\beta_1 \\
-\frac{1}{T_{\beta2}}\beta_2 \\
\dot{\psi} \\
\frac{1}{K_r}\left(-D_r\,\dot{\psi} + \varphi(\psi,\beta_1,\beta_2,\Omega_1,\Omega_2)\, L\right) \\
\frac{-R_s}{L_d}\,i_{\mathrm{d1}} + \frac{pL_q}{L_d}\,i_{\mathrm{q1}}\,\Omega_1 \\
\frac{-R_s}{L_q}\,i_{\mathrm{q1}} - \frac{pL_d}{L_q}\,i_{\mathrm{d1}}\,\Omega_1 - \frac{p\phi_f}{L_q}\,\Omega_1 \\
\frac{1}{J}\Gamma_{a1}(\beta_1,\Omega_1,\psi) - \frac{p\phi_f}{J}\,i_{\mathrm{q1}} - \frac{p(L_d-L_q)}{J}\,i_{\mathrm{d1}}\,i_{\mathrm{q1}} - \frac{f_v}{J}\,\Omega_1 \\
\frac{-R_s}{L_d}\,i_{\mathrm{d2}} + \frac{pL_q}{L_d}\,i_{\mathrm{q2}}\,\Omega_2 \\
\frac{-R_s}{L_q}\,i_{\mathrm{q2}} - \frac{pL_d}{L_q}\,i_{\mathrm{d2}}\,\Omega_2 - \frac{p\phi_f}{L_q}\,\Omega_2 \\
\frac{1}{J}\Gamma_{a2}(\beta_2,\Omega_2,\psi) - \frac{p\phi_f}{J}\,i_{\mathrm{q2}} - \frac{p(L_d-L_q)}{J}\,i_{\mathrm{d2}}\,i_{\mathrm{q2}} - \frac{f_v}{J}\,\Omega_2
\end{bmatrix} \tag{15}$$

$$g(x) = \begin{bmatrix}
\frac{1}{T_{\beta1}} & 0 & 0 & 0 & 0 & 0 & 0 & 0 & 0 & 0 \\
0 & \frac{1}{T_{\beta2}} & 0 & 0 & 0 & 0 & 0 & 0 & 0 & 0 \\
0 & 0 & 0 & 0 & \frac{1}{L_d} & 0 & 0 & 0 & 0 & 0 \\
0 & 0 & 0 & 0 & 0 & \frac{1}{L_q} & 0 & 0 & 0 & 0 \\
0 & 0 & 0 & 0 & 0 & 0 & 0 & \frac{1}{L_d} & 0 & 0 \\
0 & 0 & 0 & 0 & 0 & 0 & 0 & 0 & \frac{1}{L_q} & 0
\end{bmatrix}^T. \tag{16}$$

The both angular velocities Ω_1 and Ω_2 have not formally the same magnitude. It gives that $\lambda_1 \neq \lambda_2$, thus $\beta_1^{opt} \neq \beta_2^{opt}$. However, dynamics of angular velocity and pitch angle are different: the motion of the whole structure face the wind is slower than the adaptation of the rotation velocities of wind turbines. Ω_1, Ω_2 are controlled by the electrical inputs control V_{q1} and V_{q2}, respectively. Then, the angular speed tracking is so fast, that it shall not affected by the pitch angles variation which assumed that are included with the mechanical part. By this way, one states that

Assumption 1. The angular velocities Ω_1 and Ω_2 are the same. ■

Then, as detailed in the sequel, the both velocities are forced to be equal to a same reference value Ω^* for a given optimum tip speed ratio λ_{opt}. It is concluded that, in the current study, one has

$$\lambda_1 = \lambda_2 = \lambda \quad \text{and} \quad \beta_1^{opt} = \beta_2^{opt} = \beta^{opt}, \tag{17}$$

which gives

$$\begin{aligned}\beta_1^* &= \beta^{opt} + \Delta\beta_1 \\ \beta_2^* &= \beta^{opt} + \Delta\beta_2.\end{aligned} \tag{18}$$

Given that the rotation is made thanks to $F_{d,1}$ and $F_{d,2}$, one states a symmetric behavior, which gives $\Delta\beta_1 = -\Delta\beta_2 = \Delta\beta$. Then, one gets

$$\begin{aligned}\beta_1^* &= \beta^{opt} - \Delta\beta \\ \beta_2^* &= \beta^{opt} + \Delta\beta.\end{aligned} \tag{19}$$

Then, from Assumption 1, Eq. (11) reads as

$$\varphi = C\,\mathcal{B}\cdot\left[\beta_1 - \beta_2\right] \tag{20}$$

given that $\mathcal{A}_1 - \mathcal{A}_2 = 0$, and $\mathcal{B}_1 = \mathcal{B}_2 = \mathcal{B}$. Given that the yaw motion is made by acting the pitch angles thanks to the control input $\Delta\beta$, one

defines a new control input $\bar{u}$ as

$$\bar{u} = \begin{bmatrix} \Delta\beta & V_{d1} & V_{q1} & V_{d2} & V_{q2} \end{bmatrix}^T. \tag{21}$$

The input u is a 6×1 vector whereas $\bar{u}$ is a 5×1-vector, these both vectors being linearly linked by

$$u = \begin{bmatrix} -1 & 0 & 0 & 0 & 0 \\ 1 & 0 & 0 & 0 & 0 \\ 0 & 1 & 0 & 0 & 0 \\ 0 & 0 & 1 & 0 & 0 \\ 0 & 0 & 0 & 1 & 0 \\ 0 & 0 & 0 & 0 & 1 \end{bmatrix} \cdot \bar{u} + \begin{bmatrix} \beta_{opt} \\ \beta_{opt} \\ 0 \\ 0 \\ 0 \\ 0 \end{bmatrix}. \tag{22}$$

The input $\Delta\beta$ appears in the time derivative of the pitch angles β_1 and β_2. From (13)–(16), (21) and (22), the relative degree of the yaw angle ψ versus $\Delta\beta$ equals 3.

3. Control problem statement

The control of the SEREO TWT has to ensure optimal production of electrical power. The optimal amount of electrical production depends on the site requirements (power grids, inhabitants, ...); however, one supposes here that the objective is to produce the maximal amount of energy that can produce the both generators (twice 2 MW). In this case, the wind turbines have to be face the wind. In case of a change of wind direction, the rotation of the nacelle (Shariatpanah et al., 2013) is required, in order to maintain the optimal configuration. With SEREO structure, this configuration (optimal energy) is ensured by the combination of the MPPT and the control of the yaw angle rotation. Then, three control problems have to be managed

- Force the structure to be face the wind, *i.e.,* control $\psi - \alpha$ to 0;
- Control the angular velocities of the wind turbines, in order to optimize the electrical power, *i.e.,* control Ω_1 and Ω_2 to an "optimal" reference Ω^*;
- Control the direct currents of the both generators $i_{d,1}$ and $i_{d,2}$ in order to avoid the ripple effects on the electromagnetic torque (Ezzat, Glumineau, & Plestan, 2010), *i.e.,* force $i_{d,1}$ and $i_{d,2}$ to 0.

Note that there is a link between these first objectives: the action on the pitch angles has an influence on the optimal value of λ. A consequence is that, if the structure is not face the wind, the produced energy is not, during the transient time, *formally optimal* because the pitch angles are not optimal, but used in order to ensure the rotation.

Angular velocities control. As previously explained, the two wind turbines have to reach the maximum power coefficient, by keeping their tip-speed ratios at their optimal values, for given pitch angles of wind turbines blades. Therefore, the rotational speeds of the two wind turbines are controlled at a reference which are derived from λ_{opt} by (2). Then, recalling Assumption 1, the reference of the rotational speed reads as

$$\Omega^* = \frac{V\cos(\psi - \alpha)}{R}\lambda_{opt}. \tag{23}$$

Direct current control. The ripples of the electromagnetic torque can be increasing the fatigues loads in the mechanical shaft of the wind turbine, and affecting the produced power. In order to avoid these drawbacks, one solution consists in forcing the direct current i_d at zero. The references of the direct currents are given as (Ezzat et al., 2010; Hamida, Glumineau, & De Leon, 2012)

$$i_{d,1}^* = i_{d,2}^* = 0. \tag{24}$$

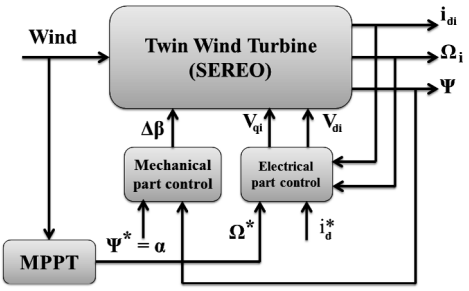

Fig. 4. Control scheme of the SEREO structure.

Control of the structure yaw rotation. When the structure is oriented face the wind, there is no difference between the drag forces ($F_{d1} - F_{d2} = 0$). If the wind direction changes, a yaw error is created (see Fig. 2); then, the rotation of the twin wind turbines is required to track the wind direction. The control objective consists in forcing $\psi - \alpha$ to 0. As said above, the rotation of the structure does not require a yaw driven motor. Therefore, the pitch angles of the two wind turbines blades are changed, in order to create a difference between the drag coefficients $C_{d,1}$ and $C_{d,2}$, *i.e.,* between the drag forces F_{d1} and F_{d2} of the both wind turbines. Thanks to this difference, a yawing torque Γ_ψ defined as

$$\Gamma_\psi = (F_{d1} - F_{d2})\, L \tag{25}$$

is appearing and forces the motion of the rotation.

Control scheme. The proposed control scheme of the SEREO structure is shown by Fig. 4.

4. Control strategy

As detailed in the previous section, the control of the twin wind turbines includes the mechanical part control of the system (yaw control) and the control of its electrical part (direct currents/angular velocities). In order to design a robust control solution, and given the nonlinear dynamics of the system, the selected control solution is based on sliding mode control approach. Indeed, since the introduction of sliding mode (Shtessel et al., 2014; Utkin, 1977; Utkin et al., 1999), this strategy has proved its efficiency widely implemented in different fields of application: electrical (Jezernik, Korelic, & Horvat, 2013; Utkin, 1993), wind energy conversion systems (Valenciaga & Puleston, 2007), pneumatic system (Girin et al., 2009; Plestan, Shtessel, Brégeault, & Poznyak, 2013).

The idea of such control strategy is to force the system trajectories to converge to a domain named sliding surface, and to be maintained on it in spite of perturbations and uncertainties, thanks to a discontinuous control input. The main features of this class of control are (Aghatehrani & Kavasseri, 2013; Traore, Plestan, Glumineau, & de Leon, 2008)

- The control input is based on the so-called sliding variable which is determined from the control objectives; from the sliding variable is defined the manifold called sliding surface;
- The control input, which is discontinuous, has to force the system trajectories to reach the sliding surface, in a finite time and in spite of the uncertainties and perturbations;
- Once the sliding surface is reached, the trajectories are evolving on it; the sliding surface is said attractive. By this way, the control objectives are fulfilled in spite of uncertainties and perturbations.

4.1. Some recalls

As previously claimed, the objective of sliding mode control is to propose, from the sliding variable, a closed-loop control law that forces

the output (control objective) y to track a trajectory y^* in spite of the uncertainties and perturbations. Consider the nonlinear system[1]

$$\begin{aligned} \dot{z} &= f_z(z) + g_z(z)\cdot \bar{u} \\ y &= h(z,t) \end{aligned} \tag{26}$$

with $z \in \mathcal{Z} \subset \mathbb{R}^n$ the state vector, $\bar{u} \in \mathbb{R}$ the control input and $y \in \mathbb{R}$ the control objective (which means that the control objective consists in forcing y to 0). $\mathcal{Z}$ is an open subset of $\mathbb{R}^n$. The vector fields $f_z(z)$ and $g_z(z)$ are uncertain.

The sliding variable $S(z,t)$ is defined from the control objective y such that

- $S(z,t) = 0$ induces $y \longrightarrow 0$;
- The relative degree of (26) with respect to S equals 1.

Then, from (26), one gets

$$\dot{S} = \Theta(z,t) + \Lambda(z,t)\cdot \bar{u}. \tag{27}$$

Assumption 2. The functions $\Theta(z,t)$ and $\Lambda(z,t)$ are bounded, $\forall z \in \mathcal{Z}$ and $t \geq 0$. Furthermore, $\Lambda(\cdot) > 0$. ■

Assumption 3. The functions $\Theta(\cdot)$ and $\Lambda(\cdot)$ read as

$$\begin{aligned} \Theta(\cdot) &= \Theta_N(\cdot) + \delta\Theta(\cdot) \\ \Lambda(\cdot) &= \Lambda_N(\cdot) + \delta\Lambda(\cdot) \end{aligned} \tag{28}$$

with Θ_N and Λ_N the nominal "well-known" parts, and $\delta\Theta$ and $\delta\Lambda$ the "uncertain" parts, of respectively the functions Θ and Λ. ■

Assumption 4. The function Λ_N is such that, $\forall z \in \mathcal{Z}$ and $t \geq 0$, there exist two positive constants Λ_N^m and Λ_N^M such that

$$0 < \Lambda_N^m \leq \Lambda_N \leq \Lambda_N^M.$$

Furthermore, the uncertain term $\delta\Lambda$ is such that, $\forall z \in \mathcal{Z}$ and $t \geq 0$,

$$\left|\frac{\delta\Lambda}{\Lambda_N}\right| \ll 1. \quad ■$$

Assumption 5. The function Θ_N is such that, $\forall z \in \mathcal{Z}$ and $t \geq 0$, there exists a positive constant Θ_N^M such that

$$|\Theta_N| < \Theta_N^M.$$

Furthermore, the uncertain term $\delta\Theta$ is such that, $\forall z \in \mathcal{Z}$ and $t \geq 0$,

$$\left|\frac{\delta\Theta}{\Theta_N}\right| \ll 1. \quad ■$$

Considering the following control law

$$\bar{u} = \frac{1}{\Lambda_N}\left(-\Theta_N + \vartheta\right) \tag{29}$$

with ϑ viewed as the new control input detailed in the sequel, one gets

$$\dot{S} = \underbrace{\left(\delta\Theta - \frac{1}{\Lambda_N}\cdot\Theta_N\delta\Lambda\right)}_{A} + \underbrace{\left(1 + \frac{1}{\Lambda_N}\cdot\delta\Lambda\right)}_{B}\vartheta. \tag{30}$$

From Assumptions 2–5, it is obvious that the functions A and B are bounded, which means that there exists positive constants A_M, B_m and B_M such that, $\forall z \in \mathcal{Z}$ and $t \geq 0$,

$$|A| \leq A_M, \qquad 0 < B_m \leq |B| \leq B_M. \tag{31}$$

The objective being to ensure $S = 0$ in a finite time, in spite of uncertainties of A and B, the control input ϑ is based on sliding mode approach (Shtessel et al., 2014; Utkin et al., 1999) and reads as

$$\vartheta = -K\,\mathrm{sign}(S)$$

with the gain K reading as

$$K > \frac{A_M + \eta}{B_m}$$

with $\eta > 0$, that allows to satisfy the so-called sliding condition $S\dot{S} \leq -\eta|S|$ which guarantees the finite time convergence of S to 0 (Shtessel et al., 2014; Utkin et al., 1999).

4.2. Sliding mode control of the twin wind turbines

The control design described above is now applied to the twin wind turbines structure described in Section 2. The control strategy is designed from the nonlinear model system given by (13). First-of-all, define the output vector

$$y = \begin{bmatrix} y_1 \\ y_2 \\ y_3 \\ y_4 \\ y_5 \end{bmatrix} = \begin{bmatrix} \psi - \alpha \\ \Omega_1 - \Omega_1^* \\ i_{d,1} \\ \Omega_2 - \Omega_2^* \\ i_{d,2} \end{bmatrix} \tag{32}$$

and recall that the control objective is to force y towards 0 (in practice, this objective is to force y towards a vicinity of 0).

Structural analysis. Analysis of system (13) with output (32) gives

- The relative degree vector (Isidori, 1999) of system (13)–(22) with output (32) and versus $\bar{u}$ (21) is $[3\ 2\ 1\ 2\ 1]^T$;
- The angle $\psi - \alpha$ and the both direct currents i_{d1} and i_{d2} are respectively controlled by $\Delta\beta$, V_{d1} and V_{d2}; concerning the both velocities Ω_1 and Ω_2, their dynamics are influenced by direct and quadratic currents—there is a coupling. However, the influence of direct currents on velocities dynamics is very limited given that the direct currents are forced at 0. Then, it can be established that the coupling is very reduced and the both velocities Ω_1 and Ω_2 are finally controlled respectively by V_{q1} and V_{q2}.

Uncertainties and perturbations. The main parameters[2] on which uncertainties have been considered, are (see Scenario 3 in the next section)

- The total inertia J,
- The yaw inertia K_r,
- The yaw dry friction D_r,

One supposes that each parameter can be written as the sum of a nominal value and an uncertain part, *i.e.*, for example, $J = J_N + \delta J$, with J_N the nominal value of the inertia, and δJ the uncertain term. Furthermore, the aerodynamic torques Γ_{a1}, Γ_{a2} and the drag forces F_{d1}, F_{d2} can be also viewed as uncertain functions, and then can be modeled as the previous parameters (nominal and uncertain terms). Finally, all the nominal parameters/functions and their associated uncertain terms are supposed to be bounded.

From the definition of y, and given that the relative degree of each component of the sliding vector has to be equal to 1, one defines the sliding variable vector as

$$S = \begin{bmatrix} S_\psi \\ S_{\Omega 1} \\ S_{d1} \\ S_{\Omega 2} \\ S_{d2} \end{bmatrix} = \begin{bmatrix} \dot{y}_1 + \lambda_{1\psi}\,\dot{y}_1 + \lambda_{2\psi}\,y_1 \\ \dot{y}_2 + \lambda_{\Omega 1}\,y_2 \\ y_3 \\ \dot{y}_4 + \lambda_{\Omega 2}\,y_4 \\ y_5 \end{bmatrix} \tag{33}$$

with $\lambda_{1\psi} = 2\,\xi\,w_n$, $\lambda_{2\psi} = w_n^2$ (with ξ, w_n respectively the damping coefficient and the natural frequency of ψ-dynamics once the sliding mode is established). $\lambda_{\Omega 1}$ and $\lambda_{\Omega 2}$ positive constants. Then, one gets

$$\dot{S} = \varphi_1(\cdot) + \varphi_2(\cdot)\cdot\bar{u} \tag{34}$$

[1] For a sake of clarity, the control strategy is described in single input–single output context.

[2] The choice has been made to evaluate the robustness on these parameters because their strongly affect dynamics of the system, and their identification are not a trivial task. Of course, the same study could have been done on other different parameters.

Table 1
Noise characteristics.

Measured variable	Noise magnitude (%)
Yaw angle ψ	5
Angular velocities Ω_1, Ω_2	2
Direct currents i_{d1}, i_{d2}	2

Table 2
PI controller parameters.

Controlled variable	Proportional gain	Integral gain
Velocities Ω_1 and Ω_2	$2.72.10^5$	$3.73.10^6$
Direct currents	0.95	10^{-4}
Yaw angle	1.5	0.05

Table 3
SCENARIO 1. PI performance for different mean wind speed.

Mean wind speed (m/s)	Max Γ_{em1} (kN.m)	STD Γ_{em1} (kN.m)	STD β_1 (°)
8	462.3	35.858	1.03
9	573.51	42.826	1.22
10.5	763.38	57.8	1.3

Table 4
SCENARIO 1. SMC performance for different mean wind speed.

Mean wind speed (m/s)	Max Γ_{em1} (kN.m)	STD Γ_{em1} (kN.m)	STD β_1 (°)
8	455.28	26.544	0.082
9	566.19	30.94	0.1
10.5	756	37.872	0.13

with functions $\varphi_1(\cdot)$ and $\varphi_2(\cdot)$ detailed in Appendix. The matrix φ_2 and its nominal value φ_{2N} are invertible if

$$\psi - \alpha \neq (\pm 2k+1)\frac{\pi}{2} \tag{35}$$

with $k \in \mathbb{N}$. This condition corresponds to the case that the wind direction is not strictly parallel to the arm linking the two wind turbines. It is easy to see that, if it is the case and from (10), the system becomes not controllable because no drag forces difference can be generated. Then, in the sequel, one supposes that condition (35) is fulfilled.

Given that each parameter can be divided in a nominal part and an uncertain one, the both matrices φ_1 and φ_2 can be written by a similar way, as a nominal part and an uncertain one (by using similar notations as previously)

$$\varphi_1 = \varphi_{1N} + \Delta\varphi_1, \qquad \varphi_2 = \varphi_{2N} + \Delta\varphi_2. \tag{36}$$

The control input $\bar{u}$ is defined as

$$\bar{u} = \left[\varphi_{2N}(.)\right]^{-1}\left[-\varphi_{1N}(.) + \vartheta\right] \tag{37}$$

which gives

$$\dot{S} = \left(\Delta\varphi_1 - \varphi_{2N}^{-1}\varphi_{1N}\Delta\varphi_2\right) + \left(I_{5\times5} + \varphi_{2N}^{-1}\Delta\varphi_2\right)\vartheta \tag{38}$$

It is reasonable to consider that the parametric uncertainties have limited magnitudes with respect to the nominal values, which gives that the term $\left(I_{5\times5} + \varphi_{2N}^{-1}\Delta\varphi_2\right)$ is a diagonally dominate matrix. It means that, thanks to the control law (37), dynamics of S is almost decoupled. Finally, the new control input reads as

$$\vartheta = \begin{bmatrix} -K_{\psi}\ \mathrm{sign}(S_{\psi}) \\ -K_{\Omega 1}\ \mathrm{sign}(S_{\Omega 1}) \\ -K_{d1}\ \mathrm{sign}(S_{d1}) \\ -K_{\Omega 2}\ \mathrm{sign}(S_{\Omega 2}) \\ -K_{d2}\ \mathrm{sign}(S_{d2}) \end{bmatrix}. \tag{39}$$

The sliding vector S converges to a vicinity of the origin in a finite time, by setting the gains sufficiently large in order to ensure the sliding condition for each component of the sliding vector.

5. Results and discussion

In order to evaluate the control of this new concept of wind turbine structure, simulations have been performed by supposing that each turbine is equipped by a 2 MW permanent magnet synchronous generator. The proposed approach control strategy is compared with a standard proportional integral controller, by evaluating different performances such as oscillations of the electromagnetic torques and mean generated power.

A white noise is considered on the main measured variables of SEREO system, such as yaw angle ψ, speeds Ω_1, Ω_2, and direct currents i_{d1}, i_{d2}. The magnitude of the noise has been fixed with respect to the nominal value of the measured variable (see Table 1).

Note that the first and second time derivatives of the output vector y (32) are estimated by a filter defined as $\frac{s}{\tau s+1}$. All these simulations have been made with Matlab/Simulink software and the main parameters of the twin wind turbines (Uehara et al., 2011) are listed in Table 10 (Appendix section).

PI controller. This controller is defined as (37), with ϑ reading as

$$\vartheta = \begin{bmatrix} K_{p\psi}S_{\psi} + K_{i\psi}\int_0^t S_{\psi}(\tau)\mathrm{d}\tau \\ K_{p\Omega_1}S_{\Omega_1} + K_{i\Omega_1}\int_0^t S_{\Omega_1}(\tau)\mathrm{d}\tau \\ K_{pd_1}S_{d_1} + K_{id_1}\int_0^t S_{d_1}(\tau)\mathrm{d}\tau \\ K_{p\Omega_2}S_{\Omega_2} + K_{i\Omega_2}\int_0^t S_{\Omega_2}(\tau)\mathrm{d}\tau \\ K_{pd_2}S_{d_2} + K_{id_2}\int_0^y S_{d_2}(\tau)\mathrm{d}\tau \end{bmatrix}. \tag{40}$$

The parameters of this controller are tuned as displayed in Table 2.

5.1. SCENARIO 1— The structure is face the wind (power optimization)

In order to check the behavior of the closed-loop system, the wind speed is modeled as

$$V = V_m + V_d$$

with V_m the mean wind speed set at 10 m/s, and V_d a time-varying term defined as a white noise. Note that, for this test, only simulation results of wind turbine 1 are displayed, those obtained for wind turbine 2 being similar.

Fig. 5 displays the pitch angle (middle) and power coefficient (bottom) with the SMC and PI controllers. The pitch angle is more affected when the structure is controlled with PI: the variations induce large oscillations around the optimal power coefficient $C_p^{opt} = 0.4$ (Table 10). Comparisons on the angular velocity and the direct current tracking are shown in Fig. 6. An efficient tracking is obtained for the two controllers. When the structure is face the wind, the turbines produce the same amount of energy (optimal power) by controlling the angular velocities.

Fig. 7 shows the comparison of the electromagnetic torque Γ_{em1} and the generated power of wind turbine 1. The generated power obtained with the controllers is compared with the optimal power (blue curve of Fig. 7—bottom) where $P_{opt} = 0.5\,\rho\,\pi\,R^2\,C_p^{opt}$ (Saravanakumar & Jena, 2015).

Comparisons are summarized in Tables 3–5. According to these tables, the SMC controller has a lowest standard deviation (STD) of Γ_{em1} and β_1: it induces reduced oscillations and then, low mechanical fatigue of the structure. Furthermore, a larger amount of energy is produced with SMC controller.

5.2. SCENARIO 2— The structure is not face the wind.

In order to take into account the fact that the system cannot face the wind, the wind speed profile is now defined as

$$V = (V_m + V_d)\cdot\cos(\psi - \alpha).$$

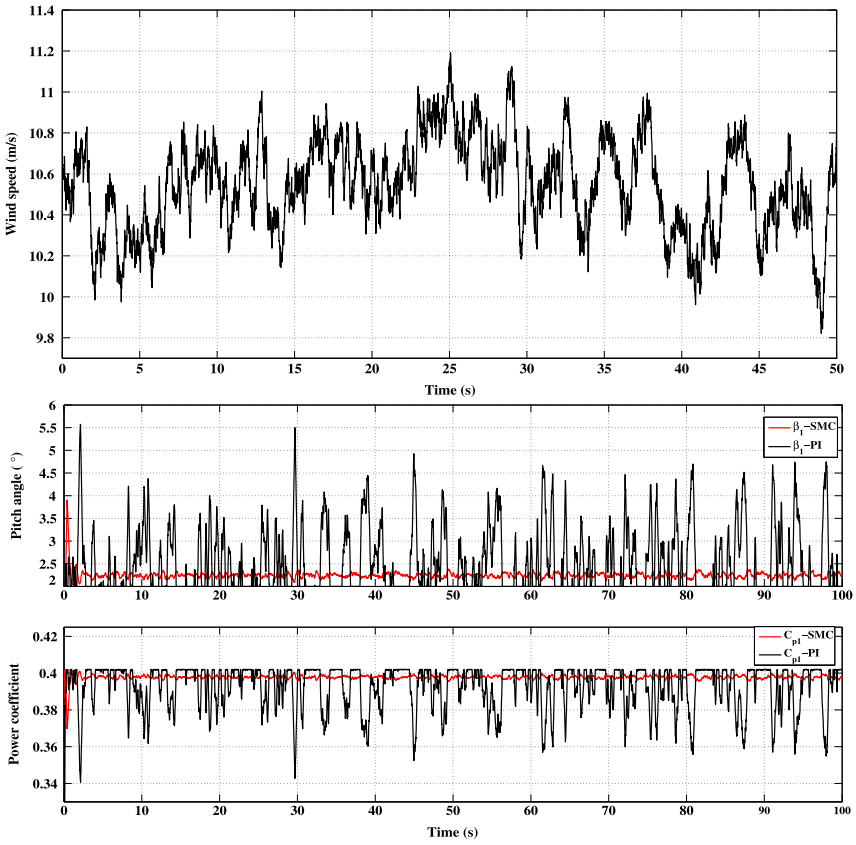

Fig. 5. SCENARIO 1. Comparison of SMC and PI controllers – Top – Wind speed (m/s). Middle —Pitch angle β_1 (°) versus time (sec). Bottom —Power coefficient C_{p1} versus time (sec).

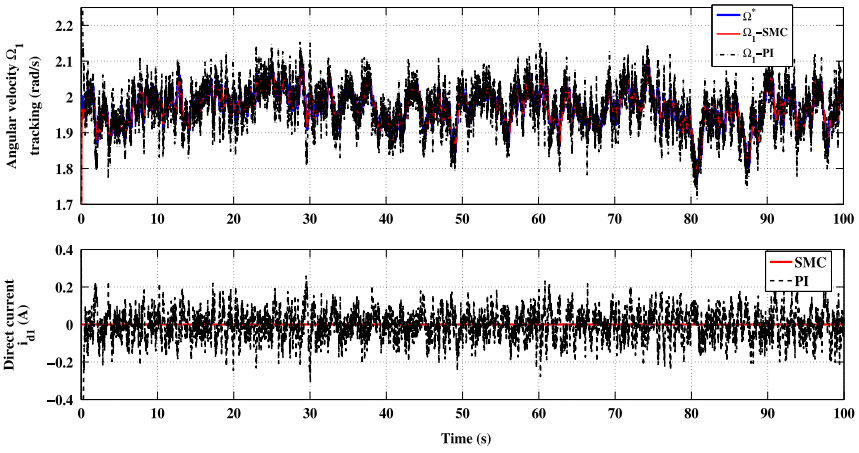

Fig. 6. SCENARIO 1. Comparison of SMC and PI – Top – Angular velocity tracking $\Omega_1 - \Omega^*$ (rad/s) versus time (sec). Bottom —Direct current i_{d1} (A) versus time (sec).

Table 5
SCENARIO 1. Performance of PI and SMC.

Mean wind speed (m/s)	Mean power PI(MW)	Mean power SMC (MW)	Difference of produced powers (kW)
8	0.5788	0.5905	11.7
9	0.8218	0.84	18.2
10.5	1.2998	1.332	32.2

Note that, when the system faces the wind, *i.e.,* $\psi = \alpha$, then one gets $V = V_m + V_d$, as used in Scenario 1. Furthermore, this wind speed definition is used for the rest of the paper. Then, the wind speed profile of Scenario 2 is the same than Scenario 1 but the direction α is changing according three values $\{0°, 10°, 30°\}$ (Fig. 8—top-left).

When the wind direction is changing, the pitch angles β_1 and β_2 are actuated (Fig. 8—middle) in order to generate drag forces difference which engenders the rotation of the whole system. The control input is displayed in Fig. 8—top-right. As shown in Fig. 8—top-left, the yaw motion is slow due to the huge SEREO mechanical structure. According

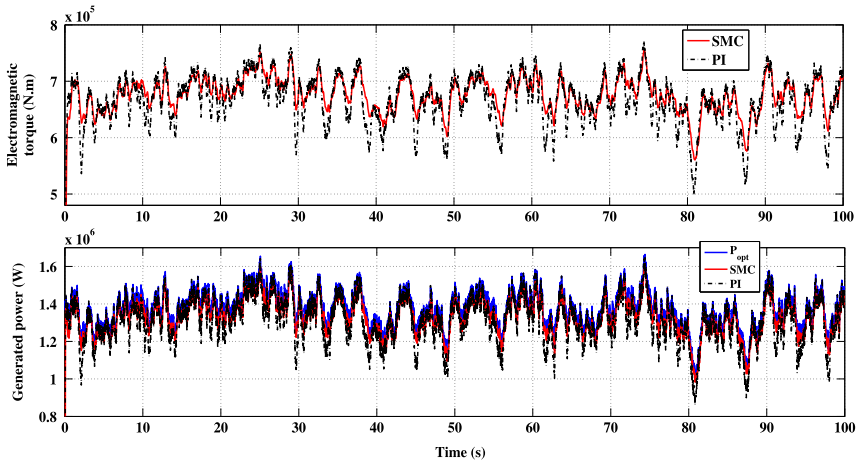

Fig. 7. SCENARIO 1. Comparison of SMC and PI – Top – Electromagnetic torque Γ_{em1} (N.m) versus time (sec). Bottom —Generated power of WT 1 (W) versus time (sec). (For interpretation of the references to color in this figure legend, the reader is referred to the web version of this article.)

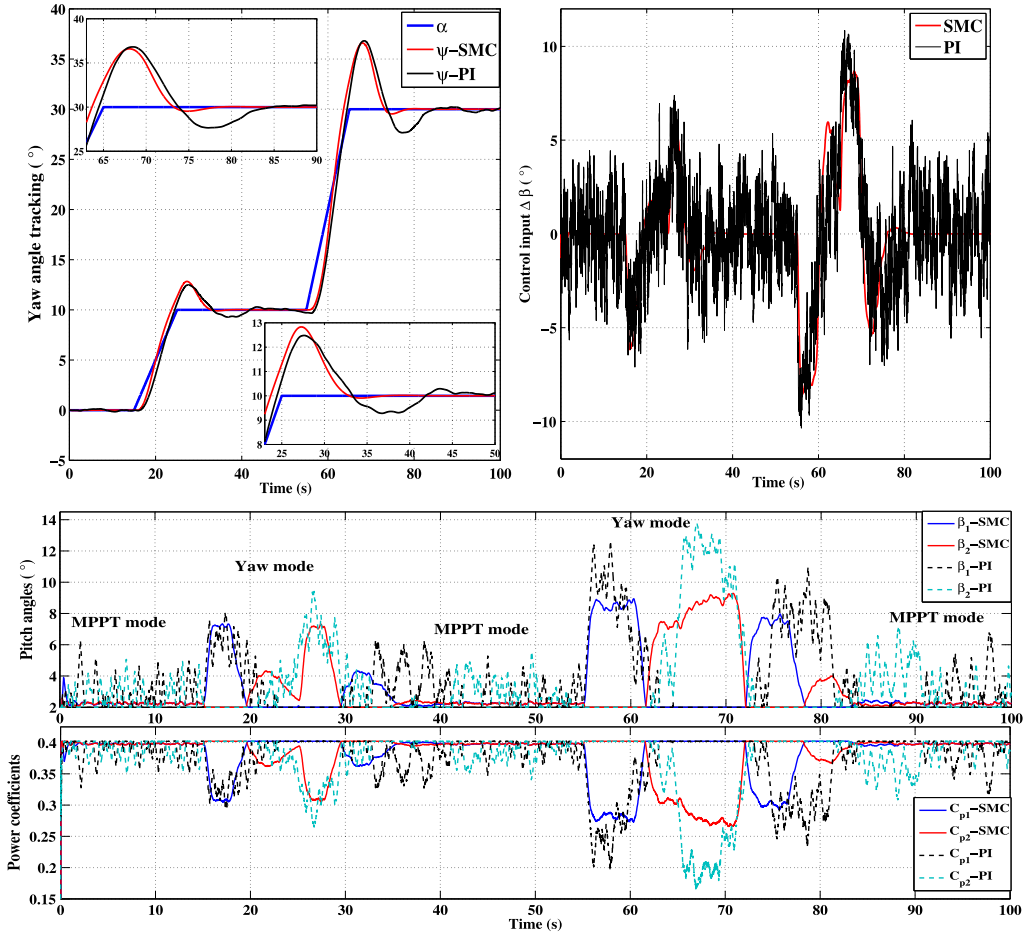

Fig. 8. SCENARIO 2. Comparison of SMC and PI – Top-left – Yaw angle tracking $\psi - \alpha$ (°) versus time (sec) . Top-right —Control input $\Delta\beta$ (°). Middle —Pitch angles β_1 and β_2 (°) versus time (sec). Bottom —Power coefficients C_{p1} and C_{p2} versus time (sec).

to the zoom (Fig. 8—top), a difference of convergence time is observed between the controllers and is smaller with SMC.

The pitch angles comparison and the power coefficients for the both turbines at **MPPT** and **yaw motion mode** are given in Fig. 8 (middle and bottom respectively). The maximum of β_1 and β_2 is higher when PI controller is applied (see Table 6), which degrades more the power coefficients. An efficient tracking of the angular velocities is obtained with the both controllers (see Fig. 9—top). The angular velocities Ω_1 and Ω_2 are not affected by the pitch variation, thanks to the fast control assured by the electrical control inputs V_{q1} and V_{q2}.

The electromagnetic torque and the generated power are compared in Fig. 9—middle and bottom. The oscillations on the drive train are evaluated with the two controllers, by measuring the STD and the maximum of Γ_{em1}, Γ_{em2} (see Table 6). In the sequel, analysis of the produced power comparison during the yaw mode is made.

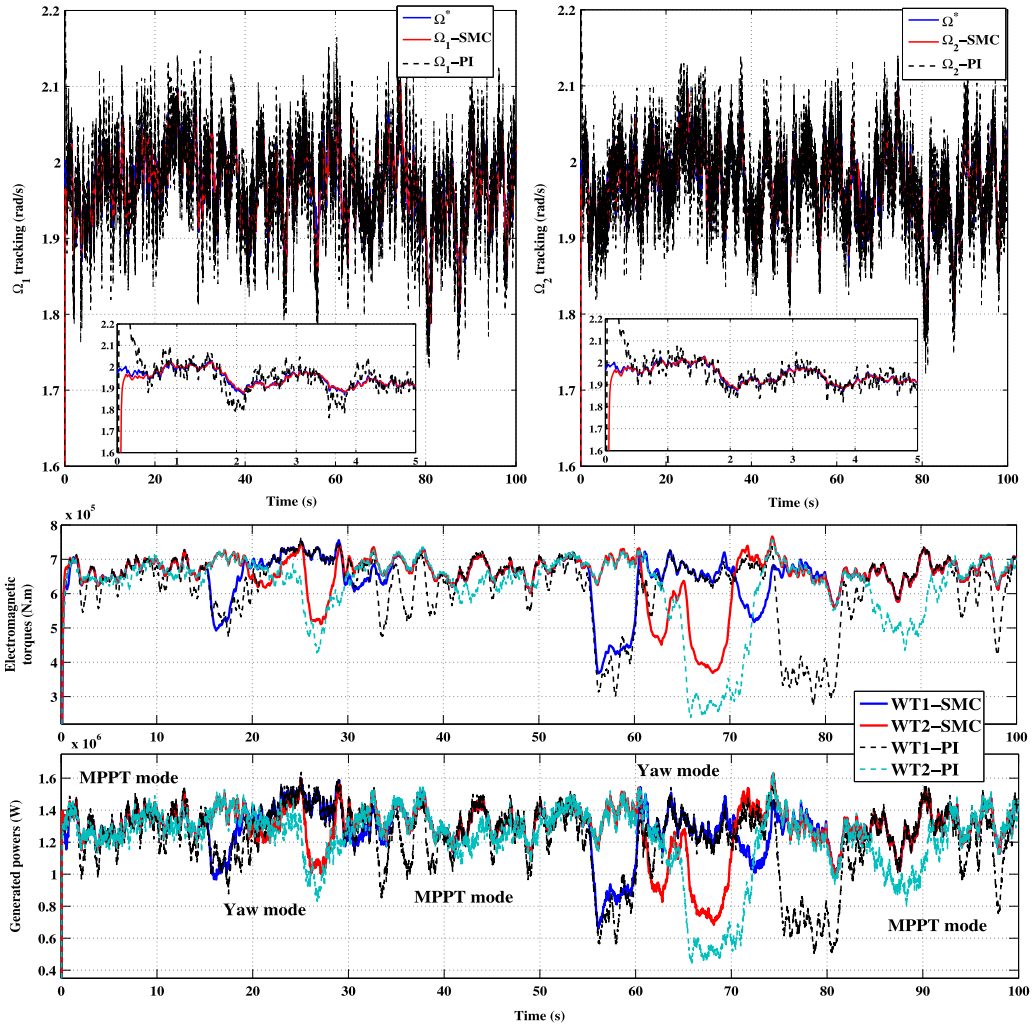

Fig. 9. SCENARIO 2. Comparison of SMC and PI - Top-left - Angular velocity tracking $\Omega_1 - \Omega^*$ (rad/s) versus time (sec). Top-right - Angular velocity tracking $\Omega_2 - \Omega^*$ (rad/s) versus time (sec). Middle - Electromagnetic torque Γ_{em1} and Γ_{em2} (N.m) versus time (sec). Bottom - Both generated powers for WT 1 and WT 2 (W) versus time (sec).

Table 6
SCENARIO 2. Performances comparison of the controllers.

	WT1		WT2	
Control strategy	PI	SMC	PI	SMC
Max Γ_{emi} (kN.m)	762.95	755.83	766.8	760
STD Γ_{emi} (kN.m)	90.25	67.6	88.735	73.437
Max β_i (°)	12.64	8.94	13.72	9.26
STD β_i (°)	2.62	1.94	2.7	1.97

Table 7
SCENARIO 2. Mean powers comparison.

	WT1	WT2
Mean power PI (MW)	1.2392	1.2391
Mean power SMC (MW)	1.2858	1.2872
Difference (kW)	46.6	48.1

Analysis of the power during the yaw mode (see Table 7). Given that the pitch angles are not optimal during the transient phase, the produced power is also not optimal. In this case, the two wind turbines do not generate the same amount of power (see Fig. 9—bottom). During the misalignment between the structure and the wind direction ($\psi - \alpha \neq 0$), the loss power is more important with PI controller as shown in Fig. 9—bottom.

Table 8
SCENARIO 3. Comparison of the controllers.

	WT1		WT2	
Control strategy	PI	SMC	PI	SMC
STD Γ_{emi} (kN.m)	107.69	79.118	111.53	85.962
Mean power (MW)	1.2103	1.2709	1.214	1.2731

5.3. SCENARIO 3 - Robustness of the control scheme.

The objective of this test is to evaluate the robustness of the controller with respect to parametric uncertainties. Scenario 3 is similar to Scenario 2 by supposing uncertainties on the yaw inertia K_r, yaw friction coefficient D_r, and total inertia (turbine + generator) J; one supposes that there are uncertainties of 20% with respect to their nominal values.

Fig. 10 and Table 8 display the main simulation results of this test.

5.4. SCENARIO 4 - Initial condition: Structure is not face the wind.

In the previous scenarios, the wind direction α and the yaw angle ψ are both initialized at the same value, *i.e.*, $\psi(0) - \alpha(0) = 0$; then, wind direction is evolving towards quite close different values (10°and 30°). In fact, these simulations have been made such that the SEREO system always starts face the wind, the idea being to check if the control structure is efficient. In Scenario 4, the wind direction is initialized at

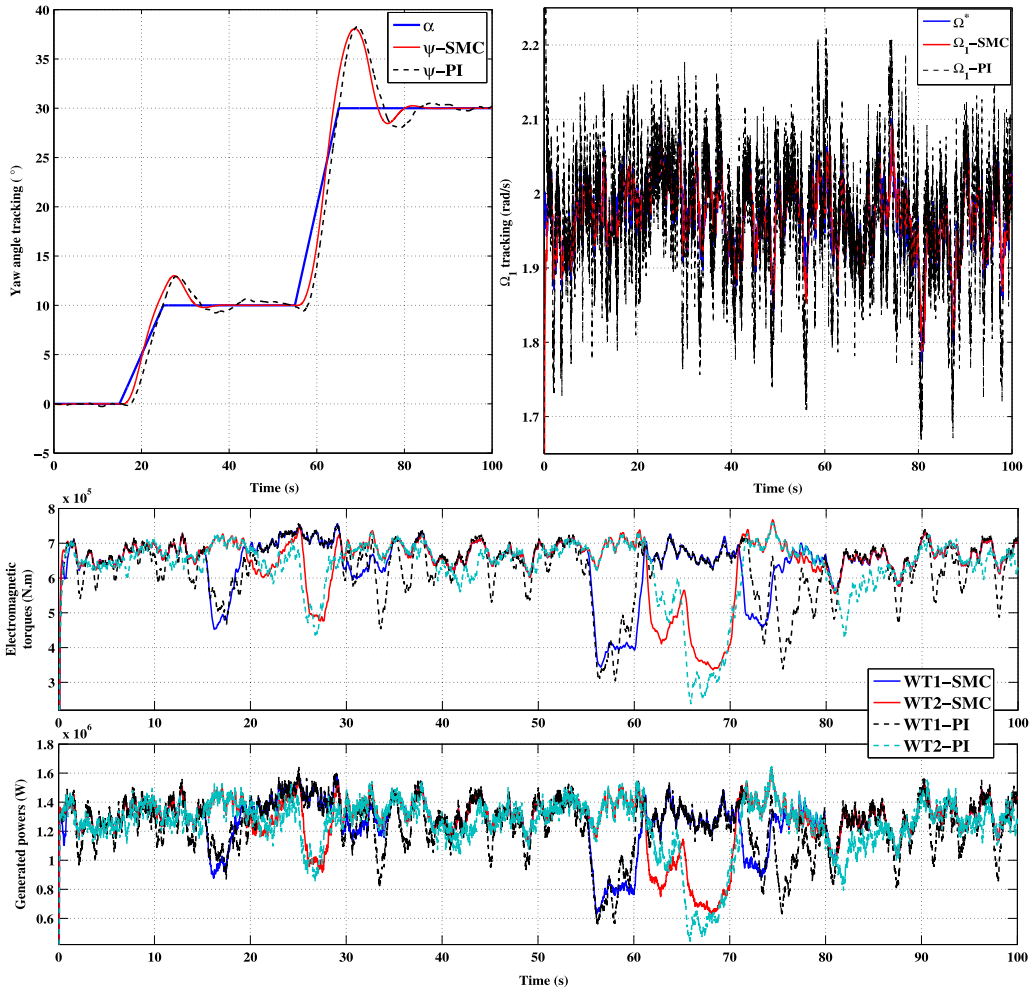

Fig. 10. SCENARIO 3. Comparison of SMC and PI – Top-left – Yaw angle tracking $\psi - \alpha$ (°) versus time (sec). Top-right —Angular speed tracking $\Omega_1 - \Omega^*$ (rad/s) versus time (sec). Middle —Electromagnetic torque Γ_{em1} and Γ_{em2} (N.m) versus time (sec). Bottom —Both generated powers for WT 1 and WT 2 (W) versus time (sec).

Table 9
SCENARIO 4. Comparison of the both controllers.

	WT1		WT2	
Control strategy	PI	SMC	PI	SMC
STD Γ_{emi} (kN.m)	147.82	116.75	148.08	122.84
Mean power (MW)	1.1268	1.2024	1.1374	1.2079

20° versus system orientation. It means that, at the initial instant, the yaw error is large comparing to Scenarios 2 and 3. Then, the turbines have to start operating even if they do not face the wind, thanks to the action on the pitch angles. The value of the wind direction $\alpha = 20°$ is maintained in order to show the time required for the SEREO system to face the wind direction. From $t = 50$ s, the wind direction changes from 20° to −20° versus structure orientation, that makes a large motion.

The results are displayed in Fig. 11, where yaw angle tracking and angular velocity Ω_1 (result of Ω_2 is being the same) is respectively shown in Fig. 11—a and b, whereas Fig. 11—c and d respectively display the electromagnetic torques and the both generated powers.

For $t \in [0, 50]s$, the both controllers make a time to force the system face the wind, due to the huge SEREO system, with a difference of 10 s between the SMC (red curve) and PI (black curve). Different amounts of power (Fig. 11-d) are produced during the yaw mode, with a larger one with SMC. Table 9 is summarizing the performances of the both controllers.

6. Conclusion and future works

A new concept of twin wind turbines has been presented in this paper: its main particularity is that there is no actuation of yaw rotation. A nonlinear model of this original structure has been given for the mechanical and electrical parts. A controller based on sliding mode concept has been designed with the objective to produce the maximum amount of power while keeping the twin wind turbines structure face the wind. The yaw rotation motion is achieved by creating a difference between the drag forces of each rotor. The proposed control strategy is compared to a standard proportional integral (PI) controller through some performance indicators as oscillations of the electromagnetic torques on the drive train and the captured power.

Future works will be focused on the conception of a more complete model of the structure including tower vibrations, aerodynamic effects, 2D or 3D wind profiles, …

Other research axes will concern the evaluation of the proposed control scheme on this full simulator, and the introduction of observers/estimators in order to estimate state or physical variables (for example, the wind velocity or direction), the objective being to go towards realistic operating conditions.

Concerning control approach, robust controllers with reduced tuning effort, as adaptive high order sliding mode controller, will be also designed and evaluated. Thanks to this evaluation, it will be checked if the gain adaptation and high order sliding mode feature can reduce the control oscillations, inducing a smoother behavior especially for the pitch with less frequent control adjustments.

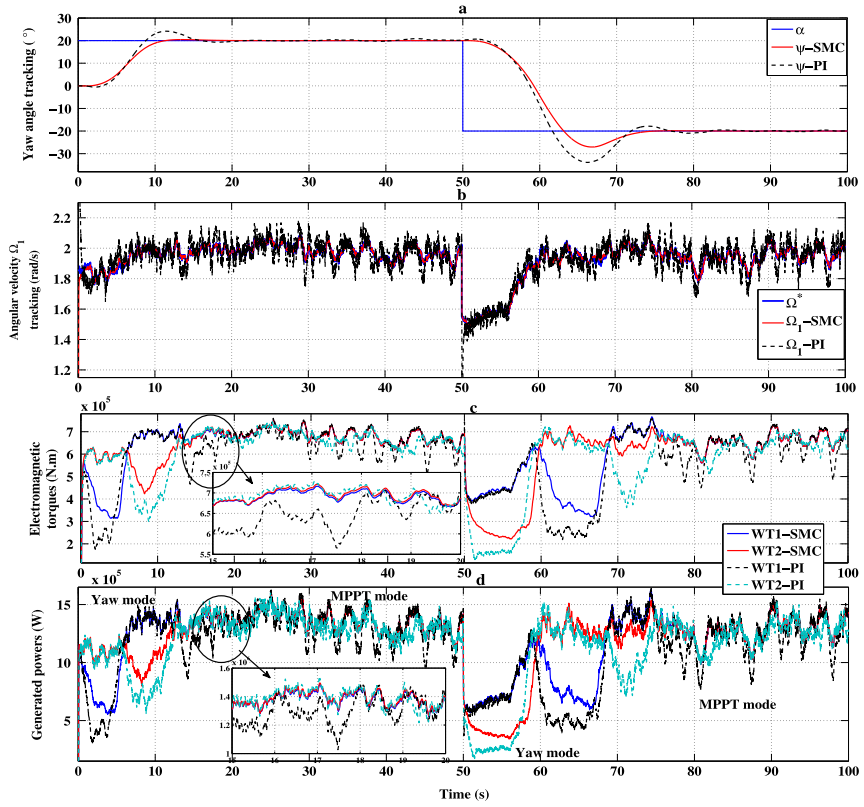

Fig. 11. SCENARIO 4. Comparison of SMC and PI – a – Yaw angle tracking $\psi - \alpha$ (°) versus time (sec). b —Angular speed tracking $\Omega_1 - \Omega^*$ (rad/s) versus time (sec). c —Electromagnetic torque Γ_{em1} and Γ_{em2} (N.m) versus time (sec). d —Both generated power for WT 1 and WT 2 (W) versus time (sec). (For interpretation of the references to color in this figure legend, the reader is referred to the web version of this article.)

Given the dimensions of the SEREO structure, it will be necessary to suppose that the wind can have different features for the both wind turbines. The control strategy will have firstly to be evaluated in such situation, and eventually to be adapted in order to maximize the power production of each turbine.

Appendix A

See Table 10.

Appendix B

The matrices φ_1 and φ_2 are detailed next page, with $f_i\ i \in \{1, 2, \dots, 7\}$ defined as

$$f_1 = \frac{p\phi_f}{J}, \qquad f_2 = \frac{p(L_d - L_q)}{J}, \qquad f_3 = \frac{R_s}{L_q}, \qquad f_4 = \frac{pL_d}{L_q},$$

$$f_5 = \frac{p\phi_f}{L_q}, \qquad f_6 = \frac{R_s}{L_d}, \qquad f_7 = \frac{pL_q}{L_d}.$$

The time derivative of the terms $\mathcal{B}$ and C appearing in the matrix $\varphi_1(\cdot)$ depend on λ, Ω, ψ, V. These derivatives are given as following

$$\begin{aligned}\dot{\mathcal{B}} &= \frac{\partial \mathcal{B}}{\partial t} = \frac{\partial \mathcal{B}}{\partial \lambda} \cdot \frac{\partial \lambda}{\partial t} = (b_1 + 2\,b_2\,\lambda \\ &\quad + 3\,b_3\,\lambda^2) \cdot \frac{\partial}{\partial t}\left(\frac{\Omega\,R}{V\,cos(\psi - \alpha)}\right) \\ &= (b_1 + 2\,b_2\,\lambda + 3\,b_3\,\lambda^2) \cdot \left(\frac{R}{V\,cos(\psi - \alpha)}\,\dot{\Omega}\right. \\ &\quad \left. + \lambda\,\mathrm{tg}(\psi - \alpha)\,\dot{\psi} - \frac{\lambda}{V}\,\dot{V}\right) \\ \dot{C} &= \frac{\partial C}{\partial t} = \frac{\partial C}{\partial V} \cdot \frac{\partial V}{\partial t} + \frac{\partial C}{\partial \psi} \cdot \frac{\partial \psi}{\partial t} \\ &= \frac{2\,C}{V}\,\dot{V} - 2\,\mathrm{tg}(\psi - \alpha)\,\dot{\psi}\end{aligned}$$

Note that the derivative of V is estimated by $\frac{s}{\tau\,s+1}$.

$$\varphi_1(.) = \begin{bmatrix} \left(\lambda_{1\psi} - \frac{D_r}{K_r}\right)\ddot{\psi} - \lambda_{1\psi}\ddot{\psi}^* + \lambda_{2\psi}\,(\dot{\psi} - \dot{\psi}^*) + \frac{CL}{K_r\,T_\beta}\,\mathcal{B}\,(\beta_1 - \beta_2)\dots \\ +\dots\frac{CL}{K_r}\,(\beta_1 - \beta_2)\,\dot{\mathcal{B}} + \frac{\mathcal{B}L}{K_r}\,(\beta_1 - \beta_2)\,\dot{C} \\ \frac{1}{J}\,\dot{\Gamma}_{a1} - (f_1 + f_2\,i_{d1})[-f_3 i_{q1} - f_4\,\Omega_1\,i_{d1} - f_5\,\Omega_1] \\ -f_2\,i_{q1}\,[-f_6\,i_{d1} + f_7\,\Omega_1\,i_{q1}]\dots \\ \dots + \left(\lambda_{\Omega 1} - \frac{f_v}{J}\right)\dot{\Omega}_1 - \lambda_{\Omega 1}\,\dot{\Omega}_1^* - \ddot{\Omega}_1^* \\ \frac{-R_s}{L_d}\,i_{d1} + \frac{P\,L_q}{L_d}\,\Omega_1\,i_{q1} \\ \frac{1}{J}\,\dot{\Gamma}_{a2} - (f_1 + f_2\,i_{d2})[-f_3 i_{q2} - f_4\,\Omega_2\,i_{d2} - f_5\,\Omega_2] \\ -f_2\,i_{q2}\,[-f_6\,i_{d2} + f_7\,\Omega_2\,i_{q2}]\dots \\ \dots + \left(\lambda_{\Omega 2} - \frac{f_v}{J}\right)\dot{\Omega}_2 - \lambda_{\Omega 2}\,\dot{\Omega}_2^* - \ddot{\Omega}_2^* \\ \frac{-R_s}{L_d}\,i_{d2} + \frac{P\,L_q}{L_d}\,\Omega_2\,i_{q2} \end{bmatrix}$$

$$\varphi_2(.) = \begin{bmatrix} \frac{-2}{K_r\,T_\beta}\,L\,C\,\mathcal{B} & 0 & 0 & 0 & 0 \\ 0 & \frac{-f_2}{L_d}\,i_{q1} & \frac{-1}{L_q}(f_1 + f_2\,i_{d1}) & 0 & 0 \\ 0 & \frac{1}{L_d} & 0 & 0 & 0 \\ 0 & 0 & 0 & \frac{-f_2}{L_d}\,i_{q2} & \frac{-1}{L_q}(f_1 + f_2\,i_{d2}) \\ 0 & 0 & 0 & \frac{1}{L_d} & 0 \end{bmatrix}.$$

Table 10
Parameters of the wind turbines.

Mechanical parameters		Parameters of PMSG	
Blade radius R	39 m	Rated power	2 MW
Air density ρ	1.205 kg/m^3	Stator resistance R_s	50 $\mu\Omega$
Rated wind speed	12 m/s	d axis inductance L_d	0.0055 H
Maximum power coefficient	0.4	q axis inductance L_q	0.00375 H
Total inertia J	10,000 kg m^2	Pole pairs number p	11
Yaw inertia K_r	$5 \cdot 10^5$ kg m^2	Field flux ϕ_f	136.25 Wb
Yaw friction coefficient D_r	200 N m/(rad/s)		
Length L	40 m		

References

Aghatehrani, R., & Kavasseri, R. (2013). Sensitivity-analysis-based sliding mode control for voltage regulation in microgrids. *IEEE Transactions on Sustainable Energy*, *4*(1), 50–57.

Beltran, B., Ahmed-Ali, T., & Benbouzid, M. (2008). Sliding mode power control of variable-speed wind energy conversion systems. *IEEE Transactions on Energy Conversion*, *23*(2), 551–558.

Beltran, B., Ahmed-Ali, T., & Benbouzid, M. (2009). High-order sliding-mode control of variable-speed wind turbines. *IEEE Transactions on Industrial Electronics*, *56*, 3314–3321.

Chen, J., Chen, J., & Gong, C. (2013). New overall power control strategy for variable-speed fixed-pitch wind turbines within the whole wind velocity range. *IEEE Transactions on Industrial Electronics*, *60*(7), 2652–2660.

Chinchilla, M., Arnaltes, S., & Burgos, J. C. (2006). Control of permanent-magnet generators applied to variable-speed wind-energy systems connected to the grid. *IEEE Transactions on Energy Conversion*, *21*(1), 130–135.

Corradini, M. L., Ippoliti, G., & Orlando, G. (2013). Robust control of variable-speed wind turbines based on an aerodynamic torque observer. *IEEE Transactions on Control Systems Technology*, *21*(4), 1199–1206.

Eberhart, P., Chung, T. S., Haumer, A., & Kral, C. (2015). Open source library for the simulation of wind power plants. In International Modelica Conference. Versaille, France.

Ezzat, M., Glumineau, A., & Plestan, F. Sensorless high order sliding mode control of permanent magnet synchronous motor. In International workshop on variable structure systems. Mexico City, Mexico, 2010.

Fridman, L., Barbot, J.-P., & Plestan, F. (2016). *New trends in sliding mode control*. London, UK: IET.

Georg, S., Schulte, H., & Aschemann, H. (2012). Control-oriented modelling of wind turbines using a Takagi-Sugeno model structure. In IEEE International Conference on Fuzzy Systems. Brisbane, Australia.

Girin, A., Plestan, F., Brun, X., & Glumineau, A. (2009). Robust control of an electropneumatic actuator: Application to an aeronautical benchmark. *IEEE Transactions on Control Systems Technology*, *17*(3), 633–645.

Glumineau, A., & de Leon-Morales, J. (2015). *Sensorless AC electric motor control robust advanced design techniques and applications*. Berlin, Germany: Springer.

Hamida, M., de Leon Morales, J., Glumineau, A., & Boisliveau, R. (2013). An adaptive interconnected observer for sensorless control of PM synchronous motors with online parameter identification. *IEEE Transactions on Industrial Electronics*, *60*(2), 739.

Hamida, M., Glumineau, A., & De Leon, J. (2012). Robust integral backstepping control for sensorless IPM synchronous motor controller. *Journal of the Franklin Institute*, *349*(5), 1734–1757.

Herskovits, A., Laffitte, O., Thome, P., & Tobie, A. V-shaped, bi-rotor wind generator on a spar floating structure, French Patent WO 2014/060 420 A1, April 24, 2012.

Huang, C., Li, F., Ding, T., Jin, Z., & Ma, X. (2015a). Second-order cone programming-based optimal control strategy for wind energy conversion systems over complete operating regions. *IEEE Transactions on Sustainable Energy*, *6*(1), 263–271.

Huang, C., Li, F., & Jin, Z. (2015b). Maximum power point tracking strategy for large-scale wind turbine dynamics. *IEEE Transactions on Industrial Electronics*, *62*(4), 2530–2539.

Ikni, D., Camara, M. S., Camara, M. B., Dakyo, B., & Gualous, H. (2014). Permanent magnet synchronous generators for large scale offshore wind farm connected to grid comparative study between dc and ac configurations. *International Journal of Renewable Energy Research*, *4*(2), 519–527.

Isidori, A. (1999). *Nonlinear control systems*. London, UK: Springer.

Jafarnejadsani, H., Pieper, J., & Ehlers, J. (2013). Adaptive control of a variable-speed variable-pitch wind turbine using radial-basis function neural network. *IEEE Transactions on Control Systems Technology*, *21*(6), 2264–2272.

Jezernik, K., Korelic, J., & Horvat, R. (2013). PMSM sliding mode FPGA-based control for torque ripple reduction. *IEEE Transactions on Power Electronics*, *28*(7), 3549–3556.

Mesemanolis, A. , & Mademlis, C. (2014). Combined maximum power point and yaw control strategy for a horizontal axis wind turbine. In International Conference on Electrical Machines. Berlin, Germany.

Munteanu, I., Bratcu, A., Cutululis, N., & Emil, C. (2008). *Advances in industrial control. Optimal control of wind energy systems*. Berlin, Germany: Springer.

Plestan, F., Shtessel, Y., Brégeault, V., & Poznyak, A. (2013). Sliding mode control with gain adaptation–application to an electropneumatic actuator. *Control Engineering Practice*, *21*(5), 679–688.

Saravanakumar, R., & Jena, D. (2015). Validation of an integral sliding mode control for optimal control of a three blade variable speed variable pitch wind turbine. *Electrical Power and Energy Systems*, *69*, 421–429.

Shariatpanah, H., Fadaeinedjad, R., & Rashidinejad, M. (2013). A new model for pmsg-based wind turbine with yaw control. *IEEE Transactions on Energy Conversion*, *28*(4), 929–937.

Shtessel, Y., Edwards, C., Fridman, L., & Levant, A. (2014). *Sliding mode control and observation*. New York, USA: Springer.

Tan, L. V., Thanh, H. N., & Dong, C. L. (2015). Advanced pitch angle control based on fuzzy logic for variable-speed wind turbine systems. *IEEE Transactions on Energy Conversion*, *30*(2), 578–587.

Tang, C. Y., Guo, Y., & Jiang, J. N. (2011). Nonlinear dual-mode control of variable-speed wind turbines with doubly fed induction generators. *IEEE Transactions on Control Systems Technology*, *19*(4), 744–756.

Traore, D., Plestan, F., Glumineau, A., & de Leon, J. (2008). Sensorless induction motor: High-order sliding-mode controller and adaptive interconnected observer. *IEEE Transactions on Industrial Electronics*, *55*(11), 3818–3827.

Uehara, A., Pratap, A., Goya, T., Senjyu, T., Yona, A., Urasaki, N., et al. (2011). A coordinated control method to smooth wind power fluctuations of pmsg-based wecs. *IEEE Transactions on Energy Conversion*, *26*(2), 550–558.

Utkin, V. (1977). Variable structure systems with sliding modes. *IEEE Transactions on Automatic Control*, *22*(2), 212–222.

Utkin, V. I. (1993). Sliding mode control design principles and applications to electrical drives. *IEEE Transactions on Industrial Electronics*, *40*(1), 23–36.

Utkin, V., Guldner, J., & Shi, J. (1999). *Sliding mode control in electro-mechanical Systems*. New York, USA: Taylor & Francis.

Valenciaga, F., & Puleston, P. (2007). Variable structure control of a wind energy conversion system based on a brushless doubly fed reluctance generator. *IEEE Transactions on Energy Conversion*, *22*(2), 499–506.

Yan, J., Lin, H., Feng, Y., Guo, X., Huang, Y., & Zhu, Z. (2012). Improved sliding mode model reference adaptive system speed observer for fuzzy control of direct-drive permanent magnet synchronous generator wind power generation system. *IET Renewable Power Generation*, *7*(1), 28–35.

Zaragoza, J., Pou, J., Arias, A., Spiteri, C., Robles, E., & Ceballos, S. (2011). Study and experimental verification of control tuning strategies in a variable speed wind energy conversion system. *Renewable Energy*, *36*(5), 1421–1430.

Zhang, Z., Zhao, Y., Qiao, W., & Qu, L. (2014). A space-vector-modulated sensorless direct-torque control for direct-drive pmsg wind turbines. *IEEE Transactions on Industry Applications*, *50*(4), 2331–2341.